Molecular Consequences of *BEST1* Gene Mutations in Canine Multifocal Retinopathy Predict Functional Implications for Human Bestrophinopathies

Karina E. Guziewicz, Julianna Slavik, Sarah J. P. Lindauer, Gustavo D. Aguirre, and Barbara Zangerl

Purpose. Bestrophin-1 gene (*BEST1*) mutations are responsible for a broad spectrum of human retinal phenotypes, jointly called bestrophinopathies. Canine multifocal retinopathy (*cmr*), caused by mutations in the dog gene ortholog, shares numerous phenotypic features with human *BEST1*-associated disorders. The purpose of this study was the assessment of molecular consequences and pathogenic outcomes of the *cmr1* ($C_{73}T/R_{25}X$) premature termination and the *cmr2* ($G_{482}A/G_{161}D$) missense mutation of the canine model compared with the $C_{87}G/Y_{29}X$ mutation observed in human patients.

Methods. Dogs carrying the *BEST1* mutation were introduced into a breeding colony and used to produce either carrier or affected offspring. Eyes were collected immediately after euthanatization at the disease-relevant ages and were harvested for expression studies. In parallel, an in vitro cell culture model system was developed and compared with in vivo results.

Results. The results demonstrate that *cmr1* and human $C_{87}G$-mutated transcripts bypass the nonsense-mediated mRNA decay machinery, suggesting the AUG proximity effect as an underlying transcriptional mechanism. The truncated protein, however, is not detectable in either species. The in vitro model accurately recapitulates transcriptional and translational expression events observed in vivo and, thus, implies loss of bestrophin-1 function in *cmr1*-dogs and $Y_{29}X$-affected patients. Immunofluorescence microscopy of *cmr2* mutant showed mislocalization of the protein.

Conclusions. Molecular evaluation of *cmr* mutations in vivo and in vitro constitutes the next step toward elucidating genotype-phenotype interactions concerning human bestrophinopathies and emphasizes the importance of the canine models for studying the complexity of the *BEST1* disease mechanism. (*Invest Ophthalmol Vis Sci.* 2011;52:4497–4505) DOI:10.1167/iovs.10-6385

From the Section of Ophthalmology, Department of Clinical Studies, School of Veterinary Medicine, University of Pennsylvania, Philadelphia, Pennsylvania.

Supported by The Foundation Fighting Blindness and by National Eye Institute/National Institutes of Health Grants EY06855, EY17549, and P30EY-001583.

Submitted for publication August 10, 2010; revised January 25 and February 22, 2011; accepted April 6, 2011.

Disclosure: **K.E. Guziewicz**, None; **J. Slavik**, None; **S.J.P. Lindauer**, None; **G.D. Aguirre**, None; **B. Zangerl**, None

Corresponding author: Barbara Zangerl, University of Pennsylvania, School of Veterinary Medicine, Ryan Veterinary Hospital, 3900 Delancey Street, Philadelphia, PA 19104-6010; bzangerl@vet.upenn.edu.

Mutations in the *BEST1* gene are an important cause of inherited retinal disorders. Hitherto, more than 100 unique allelic variants have been linked to human *BEST1* (http://www.hgmd.cf.ac.uk/) and associated with five disease phenotypes, broadly termed bestrophinopathies. Most of these sequence alterations lead to Best disease (also called Best vitelliform macular dystrophy [BVMD]), a juvenile-onset macular degeneration, characterized by abnormal accumulation of lipofuscin-like deposits in the subretinal and sub-RPE spaces and a depressed electro-oculogram light peak.[1,2] Additionally, *BEST1* mutations are associated with adult-onset foveomacular vitelliform dystrophy,[3] autosomal dominant vitreoretinochoroidopathy,[4] autosomal recessive bestrophinopathy,[5] and, as recently reported, autosomal dominant retinitis pigmentosa.[6]

Bestrophin-related phenotypes, particularly Best disease, are known for their complexity. Notably, observed pleiotropic effects of *BEST1*, together with incomplete penetrance and variable clinical expressivity, do not facilitate the dissection of the genotype-phenotype correlation, even within a single family. Consequently, disease progression and severity and the exact impact of the disease on vision impairment are difficult to predict in some BVMD-affected patients. In addition, the juvenile onset of the disease and the limited access to large sample sets make genotype-phenotype analysis an extremely challenging task.

Altered residues define three main mutation hotspots of the bestrophin-1 molecule: the highly evolutionarily conserved N-terminal part of the protein (6–30aa), the second transmembrane domain (80–105aa), and the strongly acidic region in the C terminus, immediately after the last transmembrane domain (293–312aa).[7,8] Generally, *BEST1* disease-associated mutations consist of substitutions (94%) that include nonsense changes truncating the gene product. Thus far, almost 10% of all known bestrophin-1 mutations have been linked to the multifocal vitelliform dystrophy.[9–11] Because these gene alterations have also been described in patients with classic BVMD and adult-onset foveomacular vitelliform dystrophy, the *BEST1*-related multifocal vitelliform dystrophy is considered a multifocal variant of bestrophinopathies.[7]

The *BEST1* gene product, bestrophin-1, is embedded in the basolateral plasma membrane of the retinal pigment epithelium (RPE).[12] Despite considerable controversy, several independent studies have provided persuasive evidence proving that bestrophin-1 is indeed a Ca^{2+}-dependent anion channel participating in epithelial transport across the RPE and demonstrating malfunction caused by *BEST1* mutations.[8,13–17] However, many aspects of the disease mechanism, including the impact of particular mutations on anion channel dysfunction and its correlation with the observed phenotypic variability, remain ambiguous. Extensive in vitro studies and existing rodent models have significantly contributed to a better understanding of the pathophysiology in *BEST1*-related retinopa-

thies.[18–22] However, because the laboratory-induced mouse and rat models do not replicate the human disease phenotype, it is questionable whether they could contribute to further studies on *BEST1* disease etiology or genotype-phenotype interactions or assist in the development of effective treatment strategies.

We previously described three spontaneous bestrophin-1 mutations resulting in canine multifocal retinopathy (*cmr*), an early-onset, autosomal recessive retinal disorder recognized in several dog breeds.[23,24] The distinct sequence alterations in canine *BEST1* (c*BEST1*) include a nonsense transition ($C_{73}T/R_{25}X$) located in the first coding exon (*cmr1*), a missense change ($G_{482}A/G_{161}D$) affecting a conserved glycine residue of the large intracellular loop (*cmr2*), and a frameshift mutation ($C_{1388}del/P_{463}FS$) resulting in a truncated peptide shortened by 92 C-terminal amino acids (*cmr3*). All three mutations lead to a highly consistent and similar phenotype in all *cmr*-affected dogs.[23,24] Besides the genetic basis, *cmr* shares various clinical and pathologic manifestations with human bestrophinopathies and has been proposed as a relevant animal model for studying *BEST1*-associated phenotypes.[23,24]

In the present study, we have examined the mutation responsible for *cmr1* ($R_{25}X$), a premature termination codon of the canine *BEST1*, and compared the findings to the $Y_{29}X$ early stop mutation occurring in the human ortholog gene.[25] Both mutations are positioned in the first mutational hotspot of the bestrophin-1 molecule. The ultimate goals of these studies were to characterize the bestrophin-1 null phenotype in a large, spontaneous animal model and to assess the molecular consequences of the nonsense mutation in *cmr1*-affected dogs and *BEST1*-mutated patients. In addition, the pathogenic effects of *cmr2* missense substitution have been described and compared with the *BEST1* null allele model. These evaluations provide a baseline for the future analysis of other deleterious sequence changes in the canine model with respective implications for human *BEST1* phenotypes.

Materials and Methods

Animals and Tissue Processing

Dogs carrying the *cmr1* mutation were used to produce either heterozygous or homozygous affected offspring. All animals underwent complete ophthalmic examinations, and fundus lesions were documented with fundus cameras (Genesis-D or RC-2 [Kowa Optimed, Inc., Torrance, CA]). For RNA or protein analysis, eyes were collected immediately after euthanatization at disease-relevant ages, dissected into RPE/choroid and retinal samples, frozen in liquid nitrogen, and stored at −70°C. For immunohistochemistry experiments, the enucleated globes were fixed in 4% paraformaldehyde, embedded in OCT medium, and processed as previously described.[26] All procedures complied strictly with the ARVO Statement for the Use of Animals in Ophthalmic and Vision Research.

Site-Directed Mutagenesis

Mutant clones were generated from full-length canine (c*BEST1*) or human (h*BEST1*; courtesy of Andrew R. Webster, University College London, UK) cDNA, and site-specific mutations (c*BEST1*: $-C_{73}T$, $-G_{482}A$; h*BEST1*: $-C_{87}G$) were introduced using a mutagenesis kit (QuikChange Lightning Site-Directed Mutagenesis Kit; Stratagene, La Jolla, CA) according to the manufacturer's instructions. All generated constructs were verified by direct sequencing.

In Vitro Studies

Cell Cultures. MDCK II cells (ATCC, Manassas, VA) were cultured in Eagle's minimum essential medium (EMEM; ATCC, Manassas, VA), supplemented with 10% of fetal bovine serum (FBS; Sigma-Aldrich, St. Louis, MO) and 1% of penicillin-streptomycin (Gibco Invitrogen, Grand Island, NY). HEK-293T cells (courtesy of Nicola J. Mason, University of Pennsylvania, Philadelphia, PA) were maintained in Dulbecco's minimum essential medium, low glucose (Gibco Invitrogen, Grand Island, NY), supplemented with 10% FBS (Sigma-Aldrich), and antibiotics as described. All cell lines were grown in a humidified atmosphere containing 95% air-5% CO_2 at 37°C.

Transient Transfection. For RNA and protein analyses, HEK-293T cells were seeded in six-well plates (5×10^5) and grown overnight. Transient transfection was performed at 90% cell confluence with the wild-type (WT) or mutant expression plasmids and transfection reagent (Lipofectamine 2000; Invitrogen, Carlsbad, CA) (1:5) in the presence of reduced-serum medium (OPTI-MEM I; Gibco Invitrogen, Grand Island, NY). Cell pellets were harvested 48 hours after transfection in ice-cold PBS. Each transfection experiment was carried out in triplicate, and cell pellets pooled from three wells were processed directly after harvesting. One day before transfection, MDCK cells used for immunohistochemistry experiments were re-plated on polycarbonate filters of 0.4-μm pore size (Transwell; Costar, Cambridge, MA) at 1×10^5 and allowed to grow for 3 to 4 days.[27,28] The medium was changed every other day. After reaching 90% to 95% of confluence, monolayers were washed three times with reduced-serum medium (OPTI-MEM I; Gibco Invitrogen), and the complete growth media were replaced with EMEM supplemented with 5% FBS and absence of antibiotics. For each transfection sample, wild-type or mutant expression plasmid were diluted in reduced-serum medium (OPTI-MEM I; Gibco Invitrogen) and combined with transfection reagent (Lipofectamine 2000; Invitrogen; 1:6). After 40 minutes of incubation at room temperature, formed DNA-lipid complexes were applied to each of the experimental wells. Forty-eight hours later, confluent MDCK monolayers were subjected to immunohistochemical staining. All experiments were repeated at least three times. Two additional time points after transfection (24 hours and 72 hours) were evaluated as described (data not shown).

mRNA Analysis

Total RNA was isolated from RPE/choroid or cell pellets (TRIzol; Invitrogen) and was reverse transcribed (SuperScript First-Strand Synthesis System; Invitrogen). The quality of cDNA synthesis was assessed by PCR amplification of *GAPDH*, as a housekeeping gene, using a combination of forward (5′-TGG TGC TGA GTA TGT AGT GG-3′) and reverse (5′-TGG GTG TCA CTG TTG AAG TC-3′) primers. c*BEST1* gene expression levels were evaluated with overlapping primer pairs spanning exons 2 to 7 (cBEST1_RT_F1, 5′-ATG ACC GTC ACC TAC TCA AG-3′; cBEST1_RT_R1, 5′-CAG GTA CAA CAA GGT CCA GC-3′) or exons 7 to 10 (cBEST1_RT_F2, 5′-GTT GGG CGG CAG TTC CTG AA-3′; cBEST1_RT_R2, 5′-CAA TAG GGA TCT CCG TGG CC-3′) using PCR conditions described previously.[23] Human *BEST1* primers were designed using the Web-based application Primer3 (http://frodo.wi.mit.edu/primer3/). The first primer pair (hBEST1_F1, 5′-CAT GAC CAT CAC TTA CAC AAG CC-3′; hBEST1_R1, 5′-ATC TCA TCC ACA GCC AAC AG-3′) generated a PCR product of 975 bp (annealing temperature, 60°C for 30 cycles), whereas the alternative primer set (hBEST1_F2, 5′-ATG ACC ATC ACT TAC ACA AGC CC-3′; hBEST1_R2, CTC GTA CTG GTT CCA CCA GCG GG-3′) spanned 294 bp (annealing temperature, 65°C for 30 cycles) of the human *BEST1* cDNA sequence. In both cases, the human and canine primer sets covered the region with the mutation of interest. In addition, analyzed amplicons were purified (QIAquick PCR Purification Kit; Qiagen, Valencia, CA) and sequenced in both directions (ABI 3730 sequencer; Applied Biosystems, Foster City, CA). For qRT-PCR verification, commercially available canine (Cf02697409_gH, Cf02697407_g1) or human (Hs00188249_m1) *BEST1* specific assays (TaqMan; Applied Biosystems) spanning 5′- or 3′- of the gene coding sequence were used. *ACTB* (TaqMan Gene Expression Assay, Hs03023880_g1; Applied Biosystems) was selected as a reference gene. All qRT-PCR reactions were performed in 96-well plates using a real-time PCR machine

(ABI 7500; Applied Biosystems) with detection software (7500, v2.0.1; Applied Biosystems). Relative changes in gene expression were calculated using a variation of the ΔΔCt method,[29] representing the mean across three biological replicates and respective SE (SEM bars). At least three biological replicates and three technical replicates per biological replicate were used for qRT-PCR analysis. All qRT-PCR experiments were repeated at least three times.

Protein Analysis

Protein expression level was determined by Western blot analysis according to the protocol described previously.[23] Briefly, total protein was extracted from the RPE/choroids or cell pellets in 1 mL 1× Laemmli buffer, and 40 μg extracts were run on a 4% to 15% gradient polyacrylamide gel (Bio-Rad, Hercules, CA) before they were changed to a transfer membrane (Immobilon; Millipore, Billerica, MA). The membranes were probed with mouse monoclonal anti-BEST1 antibody (sc-32792; Santa Cruz Biotechnology Inc., Santa Cruz, CA) at 1:100 dilution and were visualized with a rabbit anti-mouse IgG horseradish peroxidase secondary antibody (Zymed, Carlsbad, CA). The primary antibody used in the study (sc-32792; Santa Cruz Biotechnology), though raised against human bestrophin-1, specifically recognizes and binds to the canine C-terminal part of Best1 (Supplementary Fig. S2, http://www.iovs.org/lookup/suppl/doi:10.1167/iovs.10-6385/-/DC Supplemental), as confirmed by a series of peptide competition assay experiments using the blocking peptide (sc-22027-P; Santa Cruz Biotechnology) supplied with the antibody. Additional anti-Best1 antibodies tested (ab14929, ab2182 [Abcam, Cambridge, MA]; sc-32792, sc-22027 [Santa Cruz Biotechnology[; ab14929, NB300–164 [Novus Biologicals, Littleton, CO]; Pab-125, E6–6[12]) showed clear cross-reactivity with the canine-specific protein extracts; only ab14927 and ab14928 (Abcam, Cambridge, MA) did not cross-react with canine samples. ACTB was used as a reference protein and loading control (mouse monoclonal anti-actin, 1:10,000; Millipore, Temecula, CA). Each Western blot experiment was repeated at least three times. Relative band intensities were determined using ImageJ software (developed by Wayne Rasband, National Institutes of Health, Bethesda, MD; available at http://rsb.info.nih.gov/ij/index.html).

Immunohistochemistry

Tissue sections were washed in 1× PBS/0.25% TX-100 for 5 minutes and were blocked for 1 hour (10% normal goat serum, 1× PBS/0.25% Triton X-100, 0.05% sodium azide). Overnight incubation with 1:400 anti-BEST1 mouse monoclonal antibody (sc-32792; Santa Cruz Biotechnology) at 4°C was followed by three washes with PBS for 5 minutes each and incubation with 1:200 goat anti-mouse 568 nm Alexa Fluor (Eugene, OR) for 1 hour at room temperature. After the washes, cell nuclei were stained with DAPI for 15 minutes. Sections were coverslipped with mounting medium (Gelvatol; Sigma) after a final wash and were examined by epifluorescence microscopy (Axioplan; Carl Zeiss, Thornwood, NY).

For all in vitro studies, MDCK cell monolayers were fixed in 4% paraformaldehyde for 15 minutes, permeabilized with 0.15% TX-100 in PBS for 10 minutes, and incubated with the primary antibody, mouse monoclonal anti-BEST1 (sc-32792, 1:400; Santa Cruz Biotechnology) overnight at 4°C. For double labeling, cells were incubated simultaneously with two antibodies, anti-BEST1 (as described) and Calnexin (1:500; ab13505; Abcam) or anti-BEST1 (as described) and anti-ZO-1 (1:100; ab59720; Abcam), followed by detection with Alexa Fluor 568 goat anti-mouse and Alexa Fluor 488 goat anti-rabbit IgG, respectively, for 2 hours at room temperature. After DAPI staining and washes, filters (Transwell; Costar) were cut from the insets and mounted on microscope slides. Negative controls, nontransfected cells, mock-transfected cells, and samples without primary antibody were carried out in parallel. Each experiment was repeated at least three times.

Confocal Microscopy

Confocal images documenting the in vitro results were acquired on a tunable spectral confocal and multi-photon system (TCS-SP5; Leica Microsystems, Wetzlar, Germany) with an upright microscope (DM 6000 CFS; Leica Microsystems) through an HCX PL APO 40× (N.A. 1.25) or 60× (N.A. 1.40) oil-immersion objective. Alexa Fluor 488 and 568 were excited at 488 nm or 543 nm laser line, and emission was collected at 500 to 570 nm and 574 to 700 nm, respectively, in sequential scanning mode by the tunable internal detectors. DAPI was excited with multiphotons at 750 nm produced by a sapphire pulse laser (Chameleon Ultra II Ti; Coherent, Santa Clara, CA), and emission was collected at 380 to 500 nm. For some figures, Z stacks of a series of X-Y planes with a step size of 0.5 μm were captured.

Results

Fundus Phenotypes in *cmr* and BVMD

Canine multifocal retinopathy occurs in multiple dog breeds worldwide and manifests as bilateral multifocal areas of retinal elevations with subretinal deposits that have a tan-brown appearance (Figs. 1A1–A3). Both *cmr1*, caused by a C-to-T nonsense substitution, and *cmr2*, resulting from G-to-A missense change in c*BEST1*, result in a consistent phenotype that resembles the pathologic findings in BVMD patients (Figs. 1B1–1B3). BVMD is a clinically heterogeneous condition in which typical funduscopic changes with subretinal accumulation of egg yellow-like material predominantly affect the macular area (Fig. 1B1); in this case, the lesion is in the pseudohypopyon stage, which is also present in *cmr* (Fig. 1A2, inset[23]). However, multifocal distribution of lesions is observed in several families with autosomal dominant BVMD (Fig. 1B2) or compound heterozygous patients (Fig. 1B3). Peripheral lesions show discrepancies in number, size, and appearance and range from small and well-circumscribed yellow-white spots to large, diffuse lesions with irregular yellowish deposits, comparable to the central lesion (Figs. 1B1–1B3).

In Vivo Evaluation of the *cmr1* ($R_{25}X$) Mutation

To assess the molecular consequences of the c*BEST1* early stop mutation ($R_{25}X$), RPE tissues from wild-type, heterozygous (*cmr1*$^{+/-}$), and homozygous affected (*cmr1*$^{-/-}$) animals were evaluated at the mRNA and protein expression levels. Surprisingly, normal *BEST1* mRNA expression levels were observed in the *cmr1*-affected animals and carriers compared with the wild-type tissue (Fig. 2A). These findings were verified by qRT-PCR, and no reduction of mRNA transcript levels was noted in either *cmr1*$^{+/-}$ or *cmr1*$^{-/-}$ RPE using both qRT-PCR probes located in the 5′-end or the 3′-end of the *BEST1* cDNA sequence (Fig. 2B). On the other hand, Western blot analysis of RPE/choroid protein extracts and immunocytochemistry of retinal/RPE tissue sections clearly demonstrated a significant decrease in bestrophin-1 protein expression levels in $R_{25}X$ carriers (~50% of the wild type) and absence of the gene product in homozygous mutant animals (Figs. 2C, 2D).

cmr1 In Vitro Model

For the purpose of examining the molecular mechanism of the disease, an in vitro model system to recapitulate *cmr1* has been developed. HEK-293T cells transiently transfected with c*BEST1* wild-type or *cmr1* mutant constructs revealed the same pattern of expression, accumulating an equivalent amount of mRNA transcript, and confirming the in vivo findings (Figs. 3A, 3B). To analyze bestrophin-1 protein expression, a series of transfection studies on the MDCK epithelial cell line, grown on permeable-filter supports mimicking the physiological polarized system, were performed (Fig. 4). As illustrated in Figures 3C

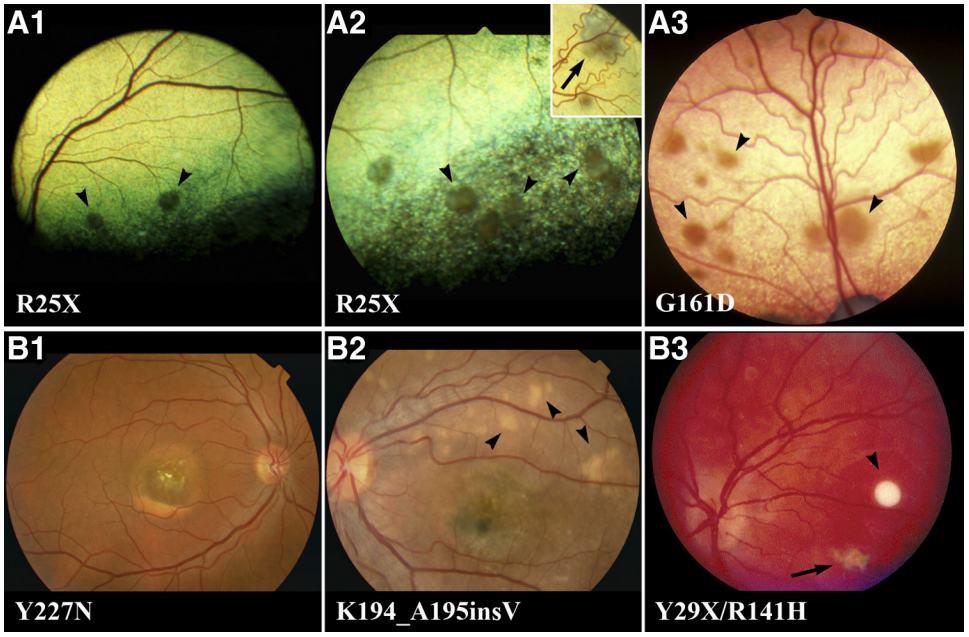

FIGURE 1. Fundus phenotypes in *cmr* and BVMD. (**A1**, **A2**) Fundus photographs of an 18-month-old English Mastiff with *cmr1* and a 15-month-old Coton de Tulear with *cmr2* (**A3**). In both animals, multiple subretinal lesions (*arrowheads*) are located in the superior tapetal region of the fundus. Note that the color of the lesions ranges from gray to tan-brown, influenced by the color of the overlying *tapetum lucidum*. (**A2**, *inset*) Fundus picture of 12-month-old Great Pyrenees with a pseudohypopyon-like lesion (*arrow*). (**B1**) Fundus appearance of a 47-year-old patient with unifocal BVMD lesion in the pseudohypopyon stage. The patient carries a $Y_{227}N$ mutation in the *BEST1* gene and has a visual acuity of 20/80. (**B2**) Multifocal BVMD (K_{194}–A_{195}insV) in a 15-year-old patient with visual acuity of 20/100; *arrowheads* indicate some of the multiple retinal lesions scattered throughout the fundus periphery. (**B3**) Fundus photograph of a 10-year-old patient with multifocal vitelliform macular dystrophy ($Y_{29}X/R_{141}H$). Irregular vitelliform degeneration is present in the fovea (*arrow*). Note the rounded, vitelliform, yolk-like degeneration superiorly (*arrowhead*) and the more subtle, somewhat diffusely demarcated, vitelliform alterations along the superior vascular arcade. Fundus photographs provided courtesy of William Beltran (**A1**, **A2**), Bruce Grahn (**A2**, *inset*), Camiel Boon (**B1**, **B2**),[11] and Patrik Schatz (**B3**).[25]

(WT) and 4C and Supplementary Figure S3 (http://www.iovs.org/lookup/suppl/doi:10.1167/iovs.10-6385/-/DCSupplemental), cells transfected with the wild-type c*BEST1* display robust, specific bestrophin-1 expression in the plasma membrane of the polarized cells. In contrast, this protein was not detectable in monolayers transfected with *cmr1* mutant plasmid (Fig. 3C). Western blot results correlated with immunocytochemistry findings, confirming the absence of bestrophin-1 in a *cmr1* in vitro model (Fig. 3D). In all cases, results were reproducible in at least three independent transfection experiments.

Canine $G_{161}D$ Missense Mutation and Its Pathogenic Effects

To compare the molecular consequences of bestrophin-1 null phenotype (*cmr1*) with the spontaneous *cmr2* missense-mutated c*BEST1* model, a series of comparable in vitro evaluations were performed. The $G_{482}A/G_{161}D$ missense mutation changes a highly evolutionarily conserved glycine residue to the polar and negatively charged aspartic acid and results in a phenotype indistinguishable from *cmr1* (Figs. 1A1–1A3[23]). At the mRNA expression level, the *cmr2* transition behaves similarly to the wild type, suggesting that mRNA stability is not altered by the guanine to adenine substitution in exon 5 of c*BEST1* (Figs. 3A, 3B). Even though Western blot analysis results do not indicate any abnormalities of the *cmr2*-affected gene product (Fig. 3D), in vitro data on the polarized model system demonstrate mislocalization of bestrophin-1 to the perinuclear space of the cells when transiently transfected with the $G_{482}A$ mutant construct (Fig. 3C). Detailed analysis revealed colocalization of *cmr2* mutant protein with Calnexin, an endoplasmic reticulum marker (Fig. 3E).

Comparison of Canine $R_{25}X$ and Human $Y_{29}X$ Mutations

To further investigate the nonsense-mediated mRNA decay insensitivity observed with *cmr1*, we examined a comparable early stop mutation ($C_{87}G/Y_{29}X$) of the h*BEST1* gene. Similar to canine $C_{73}T$, the $C_{87}G$ nonsense substitution was positioned in close proximity to the AUG-start codon, introducing a premature stop signal within the first coding exon of the human ortholog (Supplementary Fig. S1, http://www.iovs.org/lookup/suppl/doi:10.1167/iovs.10-6385/-/DCSupplemental). An h*BEST1* construct carrying the $C_{87}G$ change was created by site-directed mutagenesis and evaluated in the in vitro model system under the same conditions described for *cmr1*.

The results, summarized in Figure 5, clearly demonstrate that the $Y_{29}X$ mutation behaves in the same manner as *cmr1*. No variation in abundance of the mRNA expression level in $C_{87}G$ mutants compared with the wild-type transcript was observed when amplified by standard RT-PCR or qRT-PCR (Figs. 5A, 5B). The hypotheses of alternative start codon use, exon skipping concept, or involvement in alternative gene-splicing machinery were rejected for both canine and human *BEST1*. All PCR products spanning the region with mutations of interest corresponded to the expected sizes and were analyzed with at least two different primer pairs and confirmed by direct sequencing (data not shown).

As expected, MDCK transfected with wild-type h*BEST1* properly traffic bestrophin-1 to the cell membrane, whereas cells expressing the $Y_{29}X$-mutated variant lack the specific labeling, indicating absence of the *BEST1* protein (Fig. 5C). Similar to the canine findings, Western blot analysis supports the immunocytochemistry data (Fig. 5D), suggesting an identical mechanism underlying the $R_{25}X$ and $Y_{29}X$ mutations in dogs and humans, respectively.

DISCUSSION

Bestrophinopathies are a group of inherited retinal disorders primarily caused by point mutations scattered throughout the entire *BEST1* gene. Because of largely overlapping clinical manifestations among the *BEST1*-defined phenotypes, frequent incomplete penetrance, and, most important, markedly variable expressivity, attempts to elucidate the genotype-phenotype relationship within this group of retinopathies are diffi-

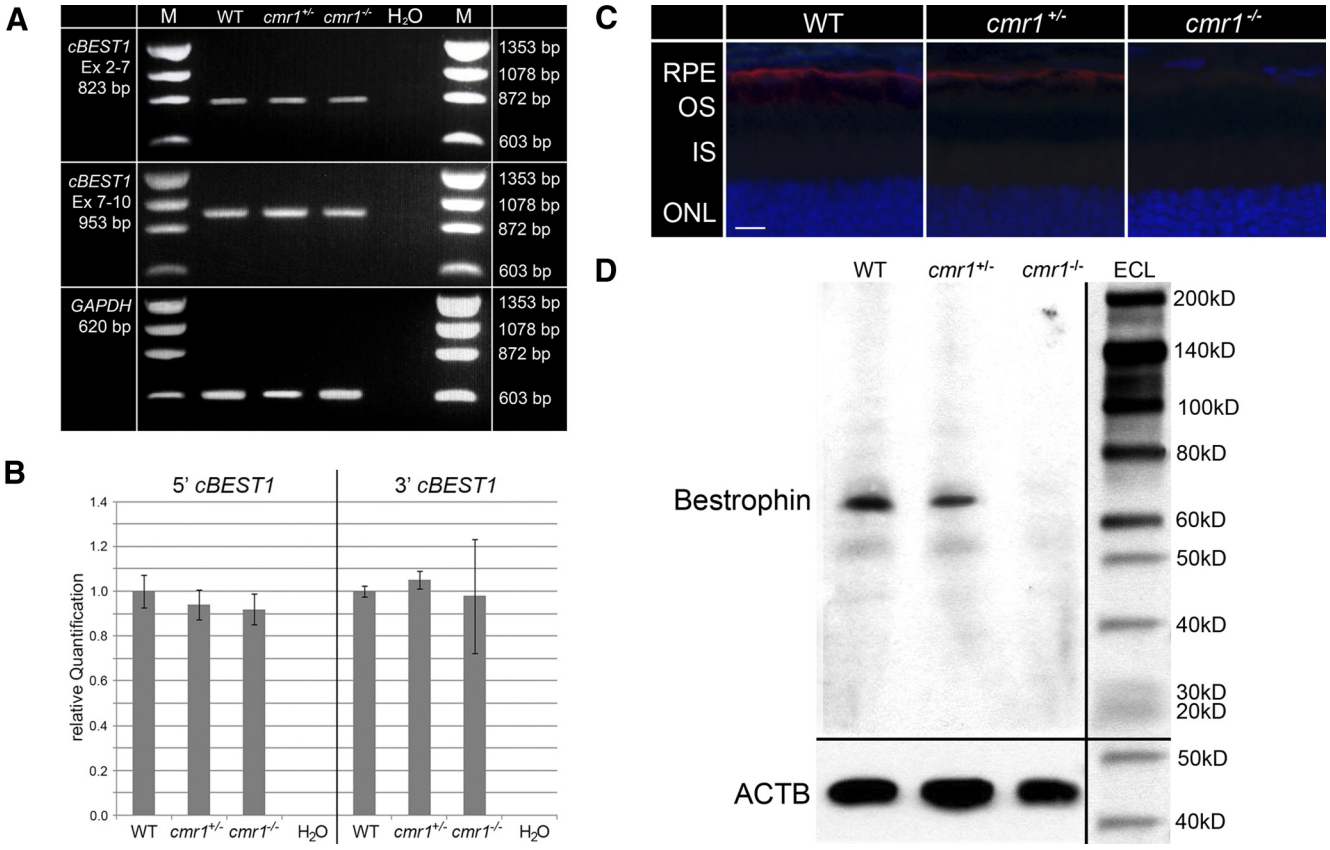

FIGURE 2. In vivo evaluation of *cmr1* premature termination mutation. (**A**) Total RNA from canine WT, *cmr1*$^{+/-}$ and *cmr1*$^{-/-}$ RPE/choroid was reverse transcribed and evaluated by RT-PCR using two overlapping primer sets corresponding to the 5′- (exon 2 − 7) or 3′- (exon 7 − 10) end of c*BEST1*. No variations in the abundance of mRNA transcripts or in amplicon sizes were noted; the control gene was *GAPDH*. (**B**) Two canine-specific *BEST1* expression assays were used for quantifying the relative RNA expression levels and validated the RT-PCR findings (*vertical bars*) SEM values. (**C**, **D**) Immunohistochemistry and Western blot analyses demonstrated twofold reduction (~50% of WT) of the bestrophin-1 protein in *cmr1*$^{+/-}$ and its absence in *cmr1*$^{-/-}$ animals. The control protein was ACTB. RPE, retinal pigment epithelium; OS, outer segment; IS, inner segment; ONL, outer nuclear layer. Scale bar, 10 μm.

cult.[10,30–32] Remarkable progress, however, has been made in establishing a link between mutated bestrophin-1 residues and the anion channel malfunction, which significantly improved our understanding of the *BEST1* disease mechanism.[6,13,19,22] Most frequently, diminished or absent Cl^- current, altered anion permeability, or defective membrane integration in association with *BEST1* nucleotide substitutions have been reported (see Refs. 7, 17 for reviews). Despite the indisputable advancements made in the elucidation of bestrophin-1 pathogenic effects, the molecular behavior of mutant transcripts and the expression of altered bestrophin-1 protein and its impact on intracellular trafficking were either not examined at all or were studied in only few cases.[6,7,17] As a result, molecular and functional consequences of *BEST1* mutations remain largely unexplored; thus, even mutations identified in early childhood do not translate to a clear prognosis. It seems, therefore, that progress in the dissection of the complex *BEST1* genotype-phenotype relationship and the establishment of a strong correlation between a particular mutation and bestrophin-1 malfunction is conditioned by recapitulating the disease phenotype in a reliable animal model.

The domestic dog represents a model that shares not only nearly half its known hereditary disorders with humans but also environmental factors and common habits. These features posit that this species is an excellent model organism for studying both monogenic and complex genetic traits.[33,34] In the past decade, use of canines as a natural model for studying inherited blinding disorders has driven this field toward the discovery of novel disease-causing mutations and substantially deepened our understanding of retinal degenerative mechanisms (see Ref. 35 for review). Moreover, the dog model has primarily contributed to the development of successful vision preservation or restoration therapies that are applicable to humans.[36–40]

Canine multifocal retinopathy is the only spontaneous large animal model available for studying the complexity of *BEST1*-associated phenotypes.[23,24] Besides having mutations in the same ortholog, *cmr* shares numerous phenotypic features with human bestrophinopathies in which multifocal along with focal-macular lesions have been documented.[5,9,11,25] Characterization of the unique *cmr1* animal model in the present study verified a *BEST1* null phenotype in which $C_{73}T/R_{25}X$ nonsense transition encodes for a truncated protein not detectable in the homozygous affected RPE or the *cmr1*-induced in vitro model. This results in the complete loss of bestrophin-1 function.

As described previously, the *cmr1* phenotype is indistinguishable from *cmr2*, the second naturally occurring canine *BEST1* model caused by the missense mutation $G_{482}A$.[23] The G-to-A substitution at the beginning of exon 5 of *cBEST1* locates the mutated amino acid residue in the large intracellular loop of the bestrophin-1 protein (106–230aa; Supplementary Fig. S1, http://www.iovs.org/lookup/suppl/doi:10.1167/iovs.10-6385/-/DCSupplemental), a region that is thus far mainly uncharacterized.[8,17] To date, 20 disease-causing mutations in h*BEST1* are reported within this region, but their molecular or functional consequences have not been examined.[7,17]

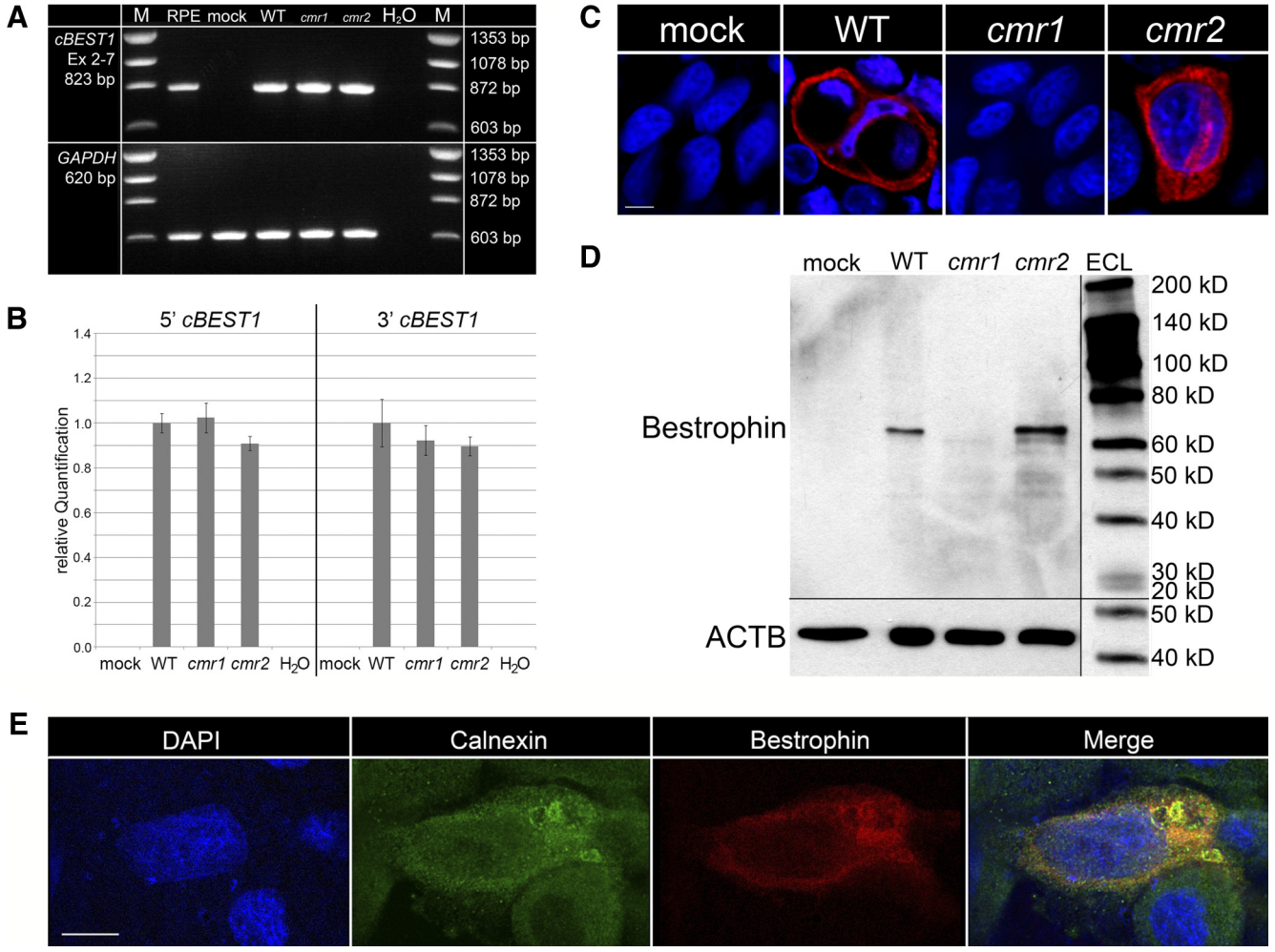

Figure 3. Canine multifocal retinopathy in vitro models. (**A**, **B**) cDNA transcripts from *cmr1* or *cmr2* transiently transfected HEK-293T cells were analyzed by RT-PCR (**A**) or qRT-PCR assays (**B**) spanning the region with mutations of interest. No c*BEST1* mRNA expression level changes were observed with either *cmr* mutant; error bars represent SEM. (**C**) Confocal images illustrating immunohistochemical detection of canine bestrophin-1 (*red*), WT, or *cmr* mutants on polarized MDCK cell monolayers. WT protein traffics to the plasma membrane of the cells, whereas the *cmr2* mutant is mislocalized. Bestrophin-1 could not be detected in cells expressing *cmr1* by either immunohistochemistry (**C**) or Western blot analysis (**D**). The in vitro model accurately recapitulates transcriptional and translational expression events observed in vivo. (**E**) Mislocalization of *cmr2* mutant protein. Fluorescence confocal images showing colocalization (*yellow-orange* in merge) of *cmr2* mutant Best1 protein (*red*) with the ER marker Calnexin (*green*). RPE, canine WT RPE/choroid tissue; mock, HEK cells mock transfected; WT, c*BEST1* WT transfected cells; *cmr1*, *cmr1* transfected cells; *cmr2*, *cmr2* construct transfected cells. The control protein was ACTB. Nuclei were labeled with DAPI (*blue*). Scale bar, 10 μm, applies to all panels.

In the *cmr2* model, the small, neutral and non-hydrophilic glycine residue at position 161 is replaced by a much larger, highly hydrophilic and negatively charged aspartic acid. We speculated that this drastic amino acid change may cause defective intracellular trafficking because of the incorrect folding of the mutant protein that cannot pass the endoplasmic

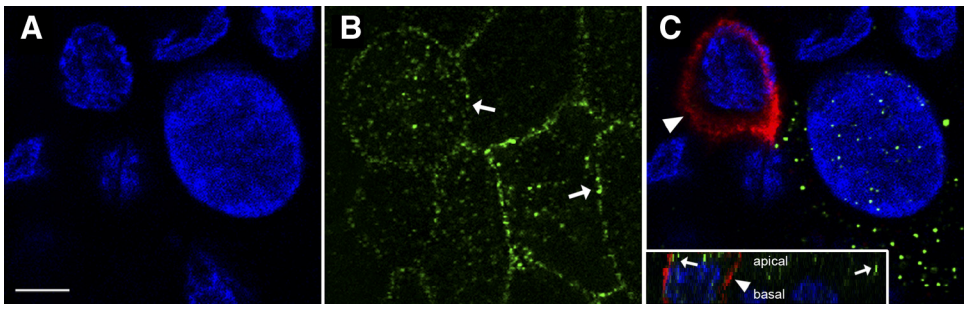

Figure 4. Cellular localization of WT bestrophin-1 in MDCK model system. Confocal images of polarized MDCK cell monolayer transfected with c*BEST1* WT and grown on Transwell filters colabeled with DAPI (**A**, *blue*), tight junction marker ZO-1 (*green*), and bestrophin-1 (*red*). Z-stack images were obtained at 0.5-μm spacing, and the representative X-Y and X-Z (**C**, *inset*) sections demonstrate protein distributions, ZO-1 (*arrows*), and bestrophin-1 (*arrowheads*) at the apical surface (**B**) or the basal side (**C**) with a total of 4-μm difference between shown images. Note the colocalization of DAPI, a nuclear counterstain, with bestrophin-1 that can only be observed toward the basal side of the polarized epithelial cells (**C**). Scale bar, 5 μm.

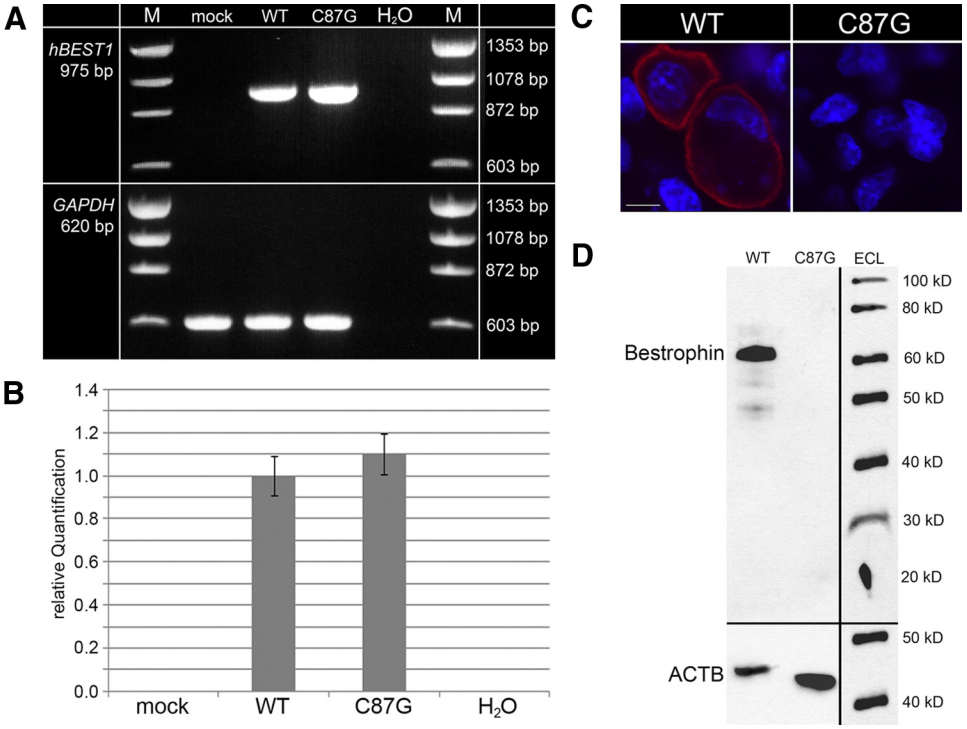

FIGURE 5. Molecular consequences of $Y_{29}X$ h*BEST1* nonsense mutation. In vitro evaluation of h*BEST1* WT and $C_{87}G$ early stop mutations at the mRNA (**A**, **B**) and protein expression (**C**, **D**) levels. (**A**) Representative gel image of h*BEST1* amplicons spanning the region with a mutation of interest. Only the predicted 975-bp product with highly comparable band intensity was present. (**B**) The expression pattern was verified by qRT-PCR, and no difference was noted between the h*BEST1* WT and mutant transcripts. Error bars represent SEM of three biological replicates. (**C**) WT human bestrophin-1 localizes to the plasma membrane of the polarized MDCK cells (*red*). The $Y_{29}X$-mutant protein was not detectable in the transfected monolayer (**C**) or by Western blot analysis (**D**). mock, HEK cells mock transfected; WT, h*BEST1* WT transfected cells; C87G, $C_{87}G$-mutant plasmid transfected cells; *GAPDH* and ACTB were used as controls. Nuclei were labeled with DAPI (*blue*). Scale bar, 10 μm.

reticulum quality control system and is subjected to degradation.[41] The fact that *cmr2*-affected bestrophin-1 protein can only be found in the endoplasmic reticulum, but not in the plasma membrane, supports our hypothesis and provides an elegant explanation of why two distinct *BEST1* mutations result in an indistinguishable phenotype. Both encode for the altered gene product that presumably results in a nonfunctional anion channel.

Nonsense mutations introducing premature termination codons (PTCs), located in the 5′ end of the gene coding sequence, are commonly considered as null allelic mutations resulting in the production of a truncated, usually inactive, protein.[42] In mammalian cells, a highly specialized surveillance pathway, termed nonsense-mediated mRNA decay (NMD), is responsible for the detection and degradation of all aberrant transcripts generated by PTCs. The NMD apparatus recognizes termination codons as premature if they are located >50 to 54 nucleotides 5′ to the final exon-exon junction (EEJ) and subjects the affected mRNAs to rapid degradation.[42,43] However, the 50- to 54-nt boundary rule has been seriously challenged in a few studies describing gene transcripts carrying PTCs and accumulating expression levels similar to the wild type, thus resistant to the NMD machinery.[44–47] In our studies, we observed the same phenomenon of NMD insensitivity occurring with the canine $C_{73}T$ and the comparable human $C_{87}G$ mutation. In both cases, the generated premature stop codons are located >50 bp upstream of the last EEJ and, hence, should represent an adequate target for NMD.

Although the molecular machinery of NMD avoidance remains largely unknown, Inacio et al.[45] proposed an AUG proximity effect as an underlying mechanism for mRNA molecules that do not undergo NMD but that contain PTCs located in the vicinity of the AUG start codon. The AUG proximity effect represents a novel parameter in the NMD complex response, blunting mRNA destabilization through the presence of a nonsense mutation at the 5′ terminus of the open reading frame, which appears to dominate the 50- to 54-nt boundary rule.[45] Our study supports the AUG proximity effect as a molecular mechanism underlying the *cmr1* and $Y_{29}X$ *BEST1* mutations and provides evidence that this NMD parameter is neither tissue nor species specific. Such factors as NMD or its resistance may contribute to the modulation of the phenotypic outcomes of the disease, originated by nonsense mutation and the variable expressivity observed in *BEST1*-related phenotypes. To our knowledge, this is the first report demonstrating the NMD resistance effect in conjunction with a retinal disease–associated gene.

The assessment of molecular and functional consequences of *cmr1* and *cmr2*, two canine models recapitulating human bestrophinopathy phenotypes, constitute the first step toward the elucidation of genotype-phenotype interactions of bestrophinopathies and indicate the importance of the canine model for studying the complexity of the disease mechanism and the development of future therapeutic approaches.

Acknowledgments

The authors thank Nicky Mason (University of Pennsylvania) for sharing cell line aliquots, Andrew Webster (University College London, UK) for providing the h*BEST1* cDNA clone, Kathleen Boesze-Battaglia and Altaf Kazi (University of Pennsylvania) for antibody aliquots and helpful suggestions, Lingli Zhang (Penn Veterinary School Core Imaging Facility, University of Pennsylvania) for excellent assistance with the confocal microscopy, Susan Grodman for contributing helpful discussions and incentive to critically review the presented work, Lydia Melnyk for editorial help, William Beltran (Section of Ophthalmology, University of Pennsylvania) and Bruce Grahn (Western College of Veterinary Medicine, University of Saskatchewan, Saskatoon, SK, Canada) for providing canine fundus photographs, and Patrik Schatz (Department of Ophthalmology, Lund University Hospital, Lund, Sweden) and Camiel Boon (Department of Ophthalmology, Radboud University Nijmegen Medical Centre, Nijmegen, Netherlands) for providing fundus photographs of affected patients and for expert advice.

References

1. Petrukhin K, Koisti MJ, Bakall B, et al. Identification of the gene responsible for Best macular dystrophy. *Nat Genet.* 1998;19:241–247.

2. Pianta MJ, Aleman TS, Cideciyan AV, et al. In vivo micropathology of Best macular dystrophy with optical coherence tomography. *Exp Eye Res.* 2003;76:203–211.
3. Seddon JM, Afshari MA, Sharma S, et al. Assessment of mutations in the Best macular dystrophy (*VMD2*) gene in patients with adult-onset foveomacular vitelliform dystrophy, age-related maculopathy, and bull's-eye maculopathy. *Ophthalmology.* 2001;108:2060–2067.
4. Yardley J, Leroy BP, Hart-Holden N, et al. Mutations of VMD2 splicing regulators cause nanophthalmos and autosomal dominant vitreoretinochoroidopathy (ADVIRC). *Invest Ophthalmol Vis Sci.* 2004;45:3683–3689.
5. Burgess R, Millar ID, Leroy BP, et al. Biallelic mutation of BEST1 causes a distinct retinopathy in humans. *Am J Hum Genet.* 2008;82:19–31.
6. Davidson AE, Millar ID, Urquhart JE, et al. Missense mutations in a retinal pigment epithelium protein, bestrophin-1, cause retinitis pigmentosa. *Am J Hum Genet.* 2009;85:581–592.
7. Boon CJ, Klevering BJ, Leroy BP, Hoyng CB, Keunen JE, den Hollander AI. The spectrum of ocular phenotypes caused by mutations in the BEST1 gene. *Prog Retin Eye Res.* 2009;28:187–205.
8. Xiao Q, Hartzell HC, Yu K. Bestrophins and retinopathies. *Pflugers Arch.* 2010;460:559–569.
9. Mullins RF, Oh KT, Heffron E, Hageman GS, Stone EM. Late development of vitelliform lesions and flecks in a patient with best disease: clinicopathologic correlation. *Arch Ophthalmol.* 2005;123:1588–1594.
10. Renner AB, Tillack H, Kraus H, et al. Late onset is common in best macular dystrophy associated with VMD2 gene mutations. *Ophthalmology.* 2005;112:586–592.
11. Boon CJ, Klevering BJ, den Hollander AI, et al. Clinical and genetic heterogeneity in multifocal vitelliform dystrophy. *Arch Ophthalmol.* 2007;125:1100–1106.
12. Marmorstein AD, Marmorstein LY, Rayborn M, Wang X, Hollyfield JG, Petrukhin K. Bestrophin, the product of the Best vitelliform macular dystrophy gene (*VMD2*), localizes to the basolateral plasma membrane of the retinal pigment epithelium. *Proc Natl Acad Sci U S A.* 2000;97:12758–12763.
13. Sun H, Tsunenari T, Yau KW, Nathans J. The vitelliform macular dystrophy protein defines a new family of chloride channels. *Proc Natl Acad Sci U S A.* 2002;99:4008–4013.
14. Tsunenari T, Sun H, Williams J, et al. Structure-function analysis of the bestrophin family of anion channels. *J Biol Chem.* 2003;278:41114–41125.
15. Strauss O, Rosenthal R. [Function of bestrophin]. *Ophthalmologe.* 2005;102:122–126.
16. Qu Z, Chien LT, Cui Y, Hartzell HC. The anion-selective pore of the bestrophins, a family of chloride channels associated with retinal degeneration. *J Neurosci.* 2006;26:5411–5419.
17. Hartzell HC, Qu Z, Yu K, Xiao Q, Chien LT. Molecular physiology of bestrophins: multifunctional membrane proteins linked to best disease and other retinopathies. *Physiol Rev.* 2008;88:639–672.
18. Rosenthal R, Bakall B, Kinnick T, et al. Expression of bestrophin-1, the product of the *VMD2* gene, modulates voltage-dependent Ca^{2+} channels in retinal pigment epithelial cells. *FASEB J.* 2006;20:178–180.
19. Yu K, Qu Z, Cui Y, Hartzell HC. Chloride channel activity of bestrophin mutants associated with mild or late-onset macular degeneration. *Invest Ophthalmol Vis Sci.* 2007;48:4694–4705.
20. Qu Z, Cheng W, Cui Y, Zheng J. Human disease-causing mutations disrupt an N-C-terminal interaction and channel function of bestrophin 1. *J Biol Chem.* 2009;284:16473–16481.
21. O'Driscoll KE, Leblanc N, Hatton WJ, Britton FC. Functional properties of murine bestrophin 1 channel. *Biochem Biophys Res Commun.* 2009;384:476–481.
22. Neussert R, Muller C, Milenkovic VM, Strauss O. The presence of bestrophin-1 modulates the Ca^{2+} recruitment from Ca^{2+} stores in the ER. *Pflugers Arch.* 2010;460:163–175.
23. Guziewicz KE, Zangerl B, Lindauer SJ, et al. Bestrophin gene mutations cause canine multifocal retinopathy: a novel animal model for best disease. *Invest Ophthalmol Vis Sci.* 2007;48:1959–1967.
24. Zangerl B, Wickström K, Slavik J, et al. Assessment of canine BEST1 variations identifies new mutations and established an independent bestrophinopathy model (cmr3) in Lapponian herders. *Mol Vis.* 2010;16:2791–2804.
25. Schatz P, Klar J, Andreasson S, Ponjavic V, Dahl N. Variant phenotype of Best vitelliform macular dystrophy associated with compound heterozygous mutations in *VMD2*. *Ophthalmic Genet.* 2006;27:51–56.
26. Beltran WA, Rohrer H, Aguirre GD. Immunolocalization of ciliary neurotrophic factor receptor alpha (CNTFRalpha) in mammalian photoreceptor cells. *Mol Vis.* 2005;11:232–244.
27. Deora AA, Gravotta D, Kreitzer G, Hu J, Bok D, Rodriguez-Boulan E. The basolateral targeting signal of CD147 (EMMPRIN) consists of a single leucine and is not recognized by retinal pigment epithelium. *Mol Biol Cell.* 2004;15:4148–4165.
28. Deora AA, Philp N, Hu J, Bok D, Rodriguez-Boulan E. Mechanisms regulating tissue-specific polarity of monocarboxylate transporters and their chaperone CD147 in kidney and retinal epithelia. *Proc Natl Acad Sci U S A.* 2005;102:16245–16250.
29. Livak KJ, Schmittgen TD. Analysis of relative gene expression data using real-time quantitative PCR and the 2(-ΔΔC(T)) Method. *Methods.* 2001;25:402–408.
30. Kramer F, White K, Pauleikhoff D, et al. Mutations in the *VMD2* gene are associated with juvenile-onset vitelliform macular dystrophy (Best disease) and adult vitelliform macular dystrophy but not age-related macular degeneration. *Eur J Hum Genet.* 2000;8:286–292.
31. Wabbels B, Preising MN, Kretschmann U, Demmler A, Lorenz B. Genotype-phenotype correlation and longitudinal course in ten families with Best vitelliform macular dystrophy. *Graefes Arch Clin Exp Ophthalmol.* 2006;244:1453–1466.
32. Boon CJ, Theelen T, Hoefsloot EH, et al. Clinical and molecular genetic analysis of best vitelliform macular dystrophy. *Retina.* 2009;29:835–847.
33. Starkey MP, Scase TJ, Mellersh CS, Murphy S. Dogs really are man's best friend—canine genomics has applications in veterinary and human medicine! *Brief Funct Genomic Proteomic.* 2005;4:112–128.
34. Schneider MR, Wolf E, Braun J, Kolb HJ, Adler H. Canine embryo-derived stem cells and models for human diseases. *Hum Mol Genet.* 2008;17:R42–R47.
35. Aguirre GD, Acland GM. Models, mutants and man: searching for unique phenotypes and genes in the dog model of inherited retinal degeneration. In: Ostrander EA, Giger U, Lindblad-Toh K, eds. *The Dog and Its Genome*. Cold Spring Harbor, NY: Cold Spring Harbor Laboratory Press; 2006:291–325.
36. Acland GM, Aguirre GD, Ray J, et al. Gene therapy restores vision in a canine model of childhood blindness. *Nat Genet.* 2001;28:92–95.
37. Tao W, Wen R, Goddard MB, et al. Encapsulated cell-based delivery of CNTF reduces photoreceptor degeneration in animal models of retinitis pigmentosa. *Invest Ophthalmol Vis Sci.* 2002;43:3292–3298.
38. Acland GM, Aguirre GD, Bennett J, et al. Long-term restoration of rod and cone vision by single dose rAAV-mediated gene transfer to the retina in a canine model of childhood blindness. *Mol Ther.* 2005;12:1072–1082.
39. Cideciyan AV, Aleman TS, Boye SL, et al. Human gene therapy for RPE65 isomerase deficiency activates the retinoid cycle of vision but with slow rod kinetics. *Proc Natl Acad Sci U S A.* 2008;105:15112–15117.
40. Komaromy AM, Alexander JJ, Rowlan JS, et al. Gene therapy rescues cone function in congenital achromatopsia. *Hum Mol Genet.* 2010;19:2581–2593.
41. Tamura T, Sunryd JC, Hebert DN. Sorting things out through endoplasmic reticulum quality control. *Mol Membr Biol.* 2010;27:412–427.
42. Lejeune F, Maquat LE. Mechanistic links between nonsense-mediated mRNA decay and pre-mRNA splicing in mammalian cells. *Curr Opin Cell Biol.* 2005;17:309–315.
43. Nagy E, Maquat LE. A rule for termination-codon position within intron-containing genes: when nonsense affects RNA abundance. *Trends Biochem Sci.* 1998;23:198–199.

44. Perrin-Vidoz L, Sinilnikova OM, Stoppa-Lyonnet D, Lenoir GM, Mazoyer S. The nonsense-mediated mRNA decay pathway triggers degradation of most BRCA1 mRNAs bearing premature termination codons. *Hum Mol Genet.* 2002;11:2805-2814.
45. Inacio A, Silva AL, Pinto J, et al. Nonsense mutations in close proximity to the initiation codon fail to trigger full nonsense-mediated mRNA decay. *J Biol Chem.* 2004;279:32170-32180.
46. Denecke J, Kranz C, Kemming D, Koch HG, Marquardt T. An activated 5′ cryptic splice site in the human ALG3 gene generates a premature termination codon insensitive to nonsense-mediated mRNA decay in a new case of congenital disorder of glycosylation type Id (CDG-Id). *Hum Mutat.* 2004;23:477–486.
47. Silva AL, Pereira FJ, Morgado A, et al. The canonical UPF1-dependent nonsense-mediated mRNA decay is inhibited in transcripts carrying a short open reading frame independent of sequence context. *RNA.* 2006;12:2160–2170.